Direct numerical simulations of the double scalar mixing layer. Part I: Passive scalar mixing and dissipation

Chong M. Cha[a)]
Aerodyne Research, Inc., 45 Manning Road, Billerica, Massachusetts 01821-3976

Stephen M. de Bruyn Kops
University of Massachusetts Amherst, Amherst, Massachusetts 01003

Mikael Mortensen
School of Aerospace, Mechanical and Mechatronic Engineering, The University of Sydney, Sydney, Australia

(Received 11 November 2005; accepted 26 April 2006; published online 30 June 2006)

The double scalar mixing layer (DSML) is a canonical problem for studying the mixing of multiple streams and, with reaction, combustion of the partially premixed type. In a DSML, a third stream consisting of a premixture of the reactants is introduced in between the pure fuel and air streams of the classic twin-feed or binary mixing problem. The well-known presumed probability density function (PDF), such as the β-PDF, can adequately model passive scalar mixing for the binary mixing problem on which state-of-the-art turbulent combustion models such as conditional moment closure and flamelet approaches rely. However, the β-PDF model, now a standard in CFD simulation, cannot describe turbulent mixing involving multiple streams; e.g., the asymmetric three-stream mixing characterizing the DSML. In this paper, direct numerical simulations of the DSML are performed to make available a high-fidelity database for developing more general, fine-scale mixing models required to compute turbulent combustion problems of practical engineering interest, which usually involve mixing between multiple streams. In this first part of two investigations, nonreacting numerical experiments are presented with emphasis on the nontrivial distributions of the passive scalar and its dissipation rate. Mapping closure modeling is applied to describe the PDFs and conditional dissipation rates of a single mixture fraction. © *2006 American Institute of Physics*. [DOI: 10.1063/1.2213887]

I. INTRODUCTION

The use of complex, multistream mixing scenarios abound in practical combustion devices such as industrial furnaces and gas turbine combustors. Increasing efficiency, reducing pollutant emissions, and enhancing performance, all while maintaining flame stability, are design challenges commonly met by novel fuel and air staging tactics. It is not uncommon to also pair such methods with partial premixing of reactant streams as done, for example, in stationary gas turbines. The partially premixed combustion modes that ensue remain as yet unmet challenges for state-of-the-art combustion models such as the flamelet,[1,2] conditional moment closure,[3,4] and transported probability density function[5,6] approaches.

A comparatively simple, illustrative example of a multistream mixing problem is the common laboratory piloted jet flame. The pilot is a partially premixed third stream set in between the fuel jet and coflowing oxidizer streams to stabilize combustion. A now famous series of such jet flames[7] forms an extensive, detailed data set used to help the further development and validation of the state-of-the-art turbulent combustion models.

To make simulations of practical flows affordable, these state-of-the-art approaches model the diffusive and reactive processes occurring at scales below the resolution of the computational grid. Of primary interest is the mixing rate of the fuel with air occurring at the unresolved scales. This can be the rate-limiting process that determines the heat release in a stably burning, nonpremixed combustion mode, or the determining process that transitions the reacting flow into combustion modes of the partially premixed or locally purely premixed type.

A normalized measure of the local fuel-to-air ratio is Bilger's well-known mixture fraction,[8]

$$\xi \equiv \frac{rY_{\mathrm{Fu}} - Y_{\mathrm{Ox}} + 1}{r+1},$$

where Y_{Fu} and Y_{Ox} are the local mass fraction of fuel and oxidizer (air), respectively, and r is the number of moles of air to fuel. By its definition, the field variable $\xi(t,\boldsymbol{x})$ is a passive scalar. Since random molecular mixing of fuel and air is described by the continuum diffusion of ξ, the scalar energy dissipation rate,

$$\chi \equiv 2\mathcal{D}\,\boldsymbol{\nabla}\xi\cdot\boldsymbol{\nabla}\xi,$$

then represents the local rate of molecular mixing of fuel with air. Here, $\mathcal{D}$ is the molecular diffusion coefficient of ξ.

[a)]Corresponding author's current address: Rolls-Royce Corporation, P. O. Box 420, Speed Code T-14, Indianapolis, IN 46206-0420. Electronic mail: Chong.M.Cha@Rolls-Royce.com

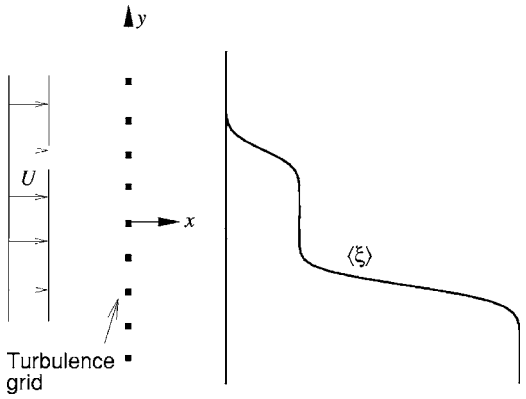

FIG. 1. Schematic of the double scalar mixing layer.

Currently, the presumed β-PDF (β probability density function) is the most commonly used computational fluid dynamics (CFD) model [(Reynolds-averaged Navier-Stokes (RANS) or large-eddy simulation] for the unresolved distribution of ξ and $\chi(\xi)$. The presumed β-PDF owes its deserved popularity to both accuracy and convenience: given the first two moments of ξ, solved for in most typical CFD computations, the two-parameter β-PDF distribution function is simple and efficient to compute and is well known to yield a fairly accurate description of the bounded, nontrivial distributions of ξ even at the early stages in a binary mixing problem. However, the β-PDF "model" has no sound physical basis and when applied to the mixing of multiple streams, cannot describe the distributions of ξ (until the mixing reaches some approximately binary mixing state).

To illustrate, consider the three-stream mixing problem represented by the double scalar mixing layer (DSML), the "simplest-but-no-simpler" problem for studying the mixing of multiple streams. In the DSML, a third "pilot" stream, a premixture of the fuel and oxidizer, is introduced in between the pure fuel ($Y_{\mathrm{Fu}}=1$ or $\xi=1$) and pure oxidizer ($Y_{\mathrm{Ox}}=1$ or $\xi=0$) feeds of the classic binary or two-stream mixing problem. In the present case, the pilot stream is premixed to $\xi=0.25$ (or $r=3$). Figure 1 shows a schematic of the mean ξ distribution in the DSML.

Figure 2 motivates the work. The figure shows, at an early stage of mixing between the three streams, the failure of the conventional β-PDF (dash-dotted lines) to describe $p_\xi(\eta)$, or equivalently, $\langle\chi|\xi=\eta\rangle$. The data (symbols) shown are from the direct numerical simulation (DNS) of the DSML. The distinguishing feature of $\langle\chi|\xi=\eta\rangle=0$ at $\eta=0.25$ shown in Fig. 2(a) is due to the pilot stream and has been recognized, for example, in large-eddy simulations of the piloted Sandia jet flame D.[9] The exact first and second moments of ξ from the DNS are used as inputs to the β-PDF model. The dashed and solid lines in 2(b) are Pope's "statistically most likely" (SML) distributions[10,11] and are described later in the paper.

The motivation of the work is to provide the necessary high-fidelity mixing data to develop the statistical fine-scale mixing models for more practical flows characterized by the mixing of multiple streams. This first part of two papers focuses on the turbulent mixing of the passive scalar field, ξ, in the DSML. (The forthcoming companion paper will consider the fine-scale mixing of the reacting scalars.) Although the fidelity of laboratory measurements, e.g., for the piloted Sandia jet flames, is rapidly approaching that of numerical simulations, they still lack the complete, detailed three-dimensional small-scale information, such as the χ fields, the knowledge of which is crucial for developing the fine-scale mixing models. Thus, DNS here is an ideal tool for the initial study of the multistream mixing problem. The DNS of the three-stream DSML has not existed until now.

In a similar DNS study of mixing, two passive scalars were considered by Juneja and Pope.[12] Under homogeneous

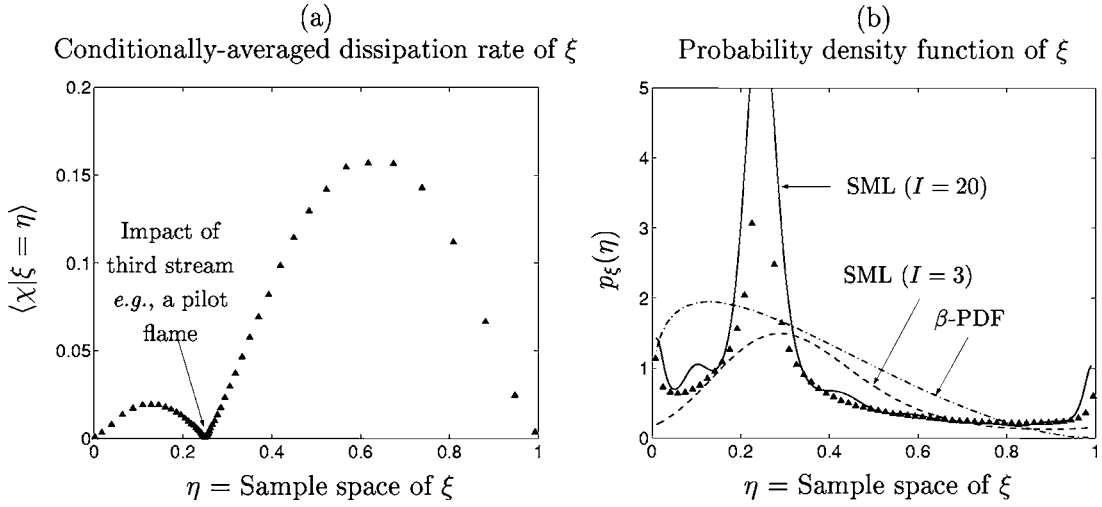

FIG. 2. Typical distributions of the dissipation rate of ξ (mixture fraction) conditionally averaged on all values of ξ (left subplot) and the corresponding probability density function of ξ (right subplot) when a third stream is introduced into the classical binary mixing problem between two streams with $\xi=0$ and $\xi=1$. The third stream here is introduced with $\xi=0.25$. Dash-dotted line shows the well-known two-parameter β-PDF constructed using the exact first and second moments ($I\equiv 2$) of the data; dashed and solid lines show the SML distribution given the exact known first three moments ($I=3$) and the first 20 moments ($I=20$). All moments are known exactly, taken from DNS. The motivation of the work is to describe multistream mixing with the least number of transport equations for the moments of ξ.

turbulence, the effect of the initial length scales and diffusivity of the scalars on the evolution of the initial "triple-delta function" joint probability density function was studied as well as the long-time, Gaussian behavior of the joint PDF. Here, we consider a nonhomogeneous case, constant Schmidt number, and focus on the early-time behavior from the triple-delta function PDF of a single passive scalar.

As a modeling objective of the present paper, the mapping closure model[13–16] is applied to develop a mixing model for an N-stream mixing problem and validated against the special case of the three-stream DNS. Past efforts in mapping closure modeling for $N>2$ streams have either considered multiple scalar mappings[17,18] or a single passive scalar with a symmetric, triple-delta function initial distribution.[19] The former approach introduces added computational overhead associated with solving the moments of each additional passive scalar and introduces new terms in the combustion modeling. Thus, the latter simpler strategy is adopted here. In Ref. 19, the focus was on the time required to reach an approximate binary mixing state for the initially symmetric three-stream case. The present work addresses the more practically relevant transition regime and also considers the general, asymmetric initial trinary (and N-ary) mixing state.

The paper is organized as follows. In the next section, the important role of p_ξ and χ in turbulent combustion modeling is reviewed. We note that this section may be skipped altogether for the reader with an advanced background in turbulent combustion modeling. In Sec. III, the DNS of the DMSL is detailed. Section IV describes the application of mapping closure to the N-stream mixing problem, motivated by results from the application of the statistically most likely distribution to the DSML. In Sec. V, the mixing stages of the DSML are delineated and behavior of the unconditional moments studied focusing on the stages of interest. The scalar probability distributions and conditional dissipation rate data are shown and compared with the mapping closure model. Section VI concludes the paper.

II. BACKGROUND

The modern turbulent combustion modeling approaches are briefly reviewed and the roles of p_ξ and χ in each of the approaches recognized. The important interdependence between these quantities is also briefly reviewed for related discussion in later sections.

In both conditional moment closure (CMC) modeling and most variants of flamelet (FL) modeling, the average mixing rate field conditional on all possible values of ξ, i.e., $\langle\chi|\xi=\eta\rangle(t,\boldsymbol{x})$, is used to obtain the conditionally averaged value of the temperature, i.e., $\langle T|\xi=\eta\rangle(t,\boldsymbol{x})$, and all the reacting scalars, e.g., $\langle Y_{\mathrm{Fu}}|\xi=\eta\rangle(t,\boldsymbol{x})$. Modeling some of the unresolved, fine-scale details of $\chi(t,\boldsymbol{x})$ is necessary and generally done by a presumed functional form of χ with ξ, or equivalently, by a presumed distribution of ξ at the unresolved scales, $p_\xi(\eta)$. In the former approach,

$$\chi \equiv \chi_0(t,\boldsymbol{x})F(\xi), \tag{1a}$$

where the function $F=\chi/\chi_0$ describes the entire dependence of χ on ξ. Note that, owing to the assumed self-similarity of F, the normalization factor χ_0 can be evaluated at a single, fixed ξ value, usually taken at the stoichiometric value of $\xi=\xi_{\mathrm{st}}$. Conditionally averaging (1a) then yields

$$\langle\chi|\xi=\eta\rangle = \langle\chi_0\rangle F(\eta). \tag{1b}$$

$F(\eta)$ is usually modeled by a presumed function derived from a laminar counterflow or mapping closure for a binary mixing problem. Kolmogorov's hypothesis that equilibrium of turbulence holds on average allows $\langle\chi_0\rangle$ ($\langle\chi\rangle$ at some specific, specified value of the mixture fraction) to be modeled by the available averaged or resolved large-scale quantities. An averaged χ relation of this kind is not always sufficient,[20,21] but provides the necessary information to solve many stably burning reacting flow problems of the nonpremixed type.

To obtain the standard, unconditional Favre averages of species concentrations and temperature in CMC and FL modeling, p_ξ is also required and is usually constructed by the generally only available first and second moments of ξ. The most commonly used form for $p_\xi(\eta)$ is the β-PDF.[22]

Presuming a probability distribution of ξ is not independent from prescribing the functional distribution for $F(\eta)$. The dependence between $p_\xi(\eta)$ and $\langle\chi|\xi=\eta\rangle$ or $F(\eta)$ can be seen explicitly within the framework of the transported probability density function (TPDF) approach for the passive scalar ξ:[23]

$$\frac{\partial}{\partial t}p_\xi(\eta,t) = -\frac{\partial}{\partial\eta}\langle\mathcal{D}\boldsymbol{\nabla}^2\xi|\xi=\eta\rangle p_\xi = -\frac{1}{2}\frac{\partial^2}{\partial\eta^2}\langle\chi|\xi=\eta\rangle p_\xi, \tag{2}$$

where homogeneity has been assumed. Equation (2) is derived from the exact continuum transport equation for ξ and thus represents the self-consistent relationship between $\langle\chi|\xi=\eta\rangle$ and $p_\xi(\eta)$, i.e., yields $p_\xi(\eta)$ given $\langle\chi|\xi=\eta\rangle$ or vice versa. For example, assuming a presumed β-PDF for ξ, (2) can be used to obtain $\langle\chi|\xi=\eta\rangle$ or $F(\eta)$ with (1a).[24,25] Note, following (2), the unique relationship between $p_\xi(\eta)$ and $\langle\chi|\xi=\eta\rangle$ is established with an initial condition for p_ξ. For more details and discussion, see Mortensen,[26] where the relationship between the PDF and the conditional dissipation (and diffusion) rate has been established for the more general, inhomogeneous case.

In TPDF modeling, to obtain $p_\xi(\eta)$ (or the more general reacting analog, $p_{\xi Y_{\mathrm{Fu}}\cdots T}$), Monte Carlo calculation techniques are usually employed.[27] In either the Eulerian or Lagrangian variants, an ensemble of "notional particles" represents the probability distribution, in the case of (2), of ξ. In a single-point framework, a micromixing model is used to account for the unresolved diffusive processes wherein the mean dissipation rate of ξ provides the physically relevant mixing time scale, e.g.,

$$T_{\mathrm{mix}} \sim \frac{\langle\xi''^2\rangle}{\langle\mathcal{D}(\boldsymbol{\nabla}\xi)^2\rangle} \equiv \frac{\langle\xi''^2\rangle}{\langle\chi\rangle/2}, \tag{3}$$

where $\langle\xi''^2\rangle$ is the variance of ξ and $\mathcal{D}$ its diffusivity. For the reacting scalars, (3) can also be used to specify the mixing time scale for all the scalars under distributed combustion;

otherwise, the conditional mean of χ is additionally required to account for flamelet combustion.[28,29]

In the current paper, a model for $\langle \chi | \xi = \eta \rangle$ to be used in CMC and FL modeling is described and tested. Additionally, for the TPDF approach, a new particle micromixing model is established for p_ξ.

III. NUMERICAL EXPERIMENT

The flow fields are assumed to satisfy the incompressible Navier-Stokes and conserved scalar transport equations

$$\nabla \cdot \boldsymbol{u} = 0, \tag{4a}$$

$$\frac{\partial \boldsymbol{u}}{\partial t} + \boldsymbol{u} \cdot \nabla \boldsymbol{u} = -\nabla p + \frac{1}{\mathrm{Re}_0} \nabla^2 \boldsymbol{u}, \tag{4b}$$

$$\frac{\partial \xi}{\partial t} + \boldsymbol{u} \cdot \nabla \xi = \frac{1}{\mathrm{Re}_0 \mathrm{Sc}} \nabla^2 \xi. \tag{4c}$$

These equations have been nondimensionalized by the initial integral length scale L_0, and the initial rms velocity u_0, so that $\mathrm{Re}_0 = \mathrm{u}_0 \mathrm{L}_0 / \nu$, where ν is the kinematic viscosity. Sc is the Schmidt number.

The flow is simulated in three dimensions using a numerical method that is discussed in detail by de Bruyn Kops and Riley.[30,31] Briefly, the transport equations for momentum and the conserved scalar are advanced in time using a third-order fractional step method with spatial derivatives computed with the pseudo-spectral technique. The nonlinear term in the momentum equation is computed in rotational form while the nonlinear term in the scalar transport equation is computed in advection and conservation form on alternate time steps to minimize aliasing.[32] Periodic boundary conditions are used in the streamwise (x) and spanwise (z) directions. Free-slip boundaries are used in the direction of the mean scalar gradient (y). The numerical domain size is $512 \times 513 \times 512$ grid points ($x \times y \times z$).

A. Velocity fields

The current simulations are designed so that the largest dynamically significant length scales are resolved, which may be important in interpreting the mixing data that are presented later in this paper. To see how, consider, for instance, Ref. 33, in which are reported the results of some carefully executed simulations, but ones that were not designed to capture the largest scales. A comparison of those results to the current results, and to laboratory data, shows that omitting the largest scales results in a faster energy decay rate and a slower growth rate in the velocity integral length scale. de Bruyn Kops and Riley[30] present a physical argument to explain these characteristics, and Wang and George[34] develop an explanation based on theory. Regardless of why the evolution of the velocity length and times scales are affected by large-scale resolution in the simulations, these characteristics affect the mixing time scale and, in particular, the time dependence of the mixing time scale. To our knowledge, Peters[35] was the first to suggest that these effects be considered when intepreting DNS data related to reacting flows.

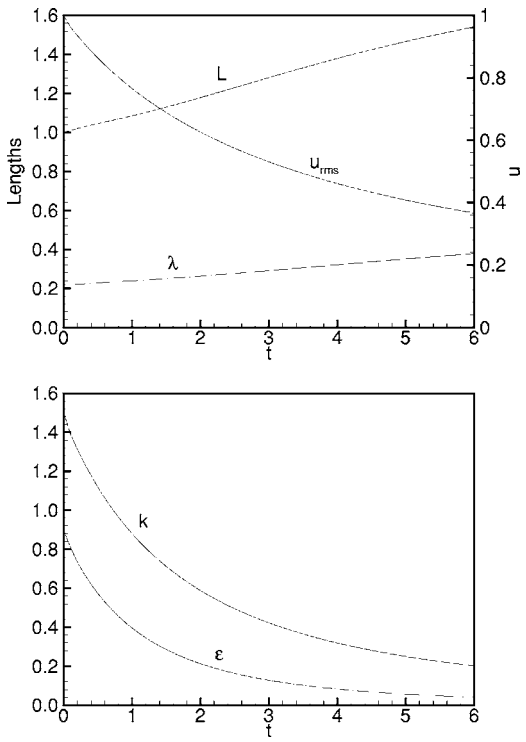

FIG. 3. The velocity integral length scale, Taylor microscale, and rms velocity versus scaled time (top); below, the turbulent kinetic energy and its dissipation rate.

In order to minimize the need for those using the current data set to be concerned with the effects of large-scale resolution on the evolution of simulated velocity fields, the velocity in the simulations has been designed to evolve like that in the classic experiment of Comte-Bellot and Corrsin[36] in homogeneous isotropic turbulence with $\mathrm{Re}_0 = 358$. Specifically, the initial velocity fields are statistically the same as those reported in Ref. 30. They are not identical because free-slip boundary conditions are used here in the direction of the mean scalar gradient, whereas periodic boundary conditions were used in the earlier simulations. As a result, the evolution of the velocity is nearly the same as, but not identical to, that reported in Ref. 30. The integral length scale (L), the Taylor microscale (λ), rms velocity (u_{rms}), turbulent kinetic energy (k), and its dissipation rate (ε) are shown in Fig. 3. Consistent with the scaling used to nondimensionalize (4), time has been scaled by the initial large-eddy turnover time L_0/u_0. To ensure that the impact of free-slip boundary conditions on the isotropy of the turbulence near the boundaries was minimal, the velocity fields between this and the periodic case were compared. The evolution of the kinetic energy and of the integral and Taylor length scales were verified to be nearly the same.

B. Scalar field

The scalar ξ is taken to be the mixture fraction ranging from zero as $y \to \infty$ to unity as $y \to -\infty$. In the initially pre-

mixed region centered about $y=0$, $\xi=0.25$. The width of this region is twice the initial velocity integral length; i.e., $L_{pm}=2$. The scalar field was allowed to evolve for six initial large-eddy turnover times in order to see the evolution of the layer after the time at which the premixed region in the initial condition ceases to have much effect on mixing and the layer has begun to act much like a single scalar layer. After the full simulation was run, the simulation was repeated from $t=0$ to $t=1.2$, with the center of mixing layer located at five different y locations, and also with the layer flipped about $y=0$ for another five simulations. This resulted in a total of ten simulations of the mixing layer using the same velocity field. The process was repeated using a statistically similar velocity field to produce another ten simulations. Furthermore, each simulation includes 512 xz planes, each of which is treated as a separate realization of the layer. Thus, the data reported for $0\leq t\leq 1.2$ are from an ensemble average of 10,240 realizations, while the data for $1.2<t\leq 6$ are from 512 realizations. The notation "$\langle\rangle$" is used to denote these ensemble averages.

In the practical applications mentioned in Sec. I, the Schmidt numbers are of order unity. The laminar values of diffusivity are not important in these applications due to their high Re. Presently, the Schmidt number in (4c) is set to $\mathrm{Sc}=0.7$ in all simulations.

Care was also taken to minimize the effect of the free-slip boundary conditions on the evolution of the scalar field. The computational domain of the DNS spans over an order of magnitude of L_0 in the nonhomogeneous, transverse direction: $-10\leq y\leq 10$. This large y domain insures that the boundary conditions do not influence the mixing. This was verified by checking that the DSML was well within the domain where the three components of the fluctuating velocity and the kinetic energy dissipation rate tensor are consistent with isotropy.

IV. MODELING

Typically, only the first two moments of ξ are calculated in a CFD simulation. Additional moment information, such as the skewness, kurtosis, and higher moments, are currently unmet modeling challenges, not to mention posing the undesirable, additional computational burden for their associated calculation. Returning to the three-stream mixing data in Fig. 2, the modeling objective is then to describe the small-scale mixing with the minimal number of large-scale equations for the statistical moments while, ideally, maintaining the computational convenience that presumed distributions like the β-PDF grants; e.g., a direct, algebraic, or analytical formula for p_ξ.

We first show that a model based on statistical inference alone, in similar fashion to the β-PDF model, cannot meet the modeling objective. Pope's "statistically most likely" (SML) distribution can be employed to illustrate the large number of moments necessary to describe the three-stream mixing statistics shown in Fig. 2. Briefly, the most likely (or least biased), statistical distribution with I given moments corresponds to the maximum "entropy" of the probability distribution, since the I given moments corresponds to the only given (or minimal) information of p_ξ. Applied to the present case, the entropy of p_ξ can be written as

$$H[p_\xi(\eta)] = -\int p_\xi(\eta)\log[\sigma p_\xi(\eta)]d\eta.$$

[For convenience, the distribution of ξ is considered rather than the standardized $(\xi-\langle\xi\rangle)/\sigma$.] Pope's SML distribution is then obtained by maximizing H with the given, first I moments of ξ as constraints:

$$p_\xi(\eta) = \frac{1}{\sigma}\exp\sum_{i=0}^{I} C_i\eta^i, \tag{5a}$$

$$0 = \int \eta^n p_\xi(\eta)d\eta - \langle\xi^n\rangle \quad \text{for } n=0,\ldots,I. \tag{5b}$$

Substitution of (5a) into (5b) and approximating the integral with the discrete trapezoidal rule yields an algebraic equation of the form $\boldsymbol{f}(\boldsymbol{C})=0$, the roots of which yield the coefficients $\boldsymbol{C}=[C_0\cdots C_I]^T$ in (5a), the SML model for p_ξ. Details can be found in Ref. 37.

Returning to Fig. 2, the dashed line in subplot (b) shows the SML distribution given the exact, first $I=3$ moments of ξ from the DNS. For $I=2$, the SML distribution gives comparable estimates as the β-PDF (see also Ref. 11). The solid line in subplot (b) shows that even the most likely distribution with minimal information given by the first $I=20$ moments of ξ is arguably insufficient to describe the shape of p_ξ. Obviously, a model requiring this many statistical moments would also not be practical.

A. Mapping closure

The mapping closure model of Chen *et al.*[13] is instead applied to describe the fine-scale statistics for the multi-stream mixing problem. Briefly, in the mapping closure approach, the statistics of a stochastic field variable (ξ in this case) is modeled by a deterministic mapping function X from a "reference field" ψ whose statistics are known, usually taken as a Gaussian field. The PDF of ξ can then be determined from

$$p_\xi(\eta,t) = \left(\frac{\partial X}{\partial\phi}\right)^{-1} p_\psi(\phi), \tag{6}$$

where $p_\psi(\phi)=(2\pi)^{-1/2}\exp(-\phi^2/2)$ for the case of a standardized Gaussian reference field. The mapping $\xi=X(\phi,t)$ is determined from the exact transport equation of ξ. For homogeneous turbulence, Gao[38] has derived the general solution

$$X(\phi,\tau) = \frac{1}{a\sqrt{2\pi}}\int_{-\infty}^{\infty} X(u,0)\exp\left[-\frac{(\phi e^{-\tau}-u)^2}{2a^2}\right]du, \tag{7}$$

where $a^2\equiv 1-e^{-2\tau}$, $\tau=\langle\mathcal{D}(\nabla\psi)^2\rangle t$ (since $\langle\psi^2\rangle\equiv 1$), and $X(\phi,0)$ is the initial condition.

Application of (7) to multiple scalar mixing can be done by formulating $X(\phi,0)$ for an initially segregated state of $N\geq 2$ scalars. The initial PDF is then

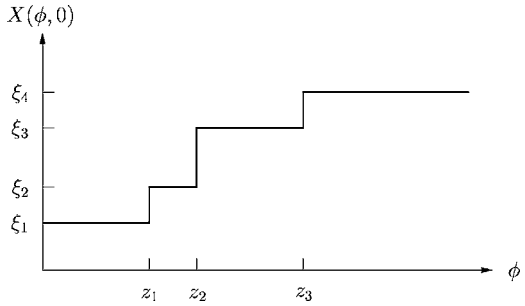

FIG. 4. Initial condition for the mapping function.

$$p_\xi(\eta,0)=\sum_{n=1}^{N} D_n\delta(\eta-\xi_n), \tag{8}$$

where $\delta(x)$ represents the Dirac delta function and D_n the relative mass of $\xi=\xi_n$ in the system; i.e., $\Sigma_{n=1}^{N}D_n=1$. The initial mapping function is then a sum of Heaviside functions $H(x)$,

$$X(\phi,0)=\xi_1+\sum_{n=2}^{N}(\xi_n-\xi_{n-1})H(\phi-z_{n-1}), \tag{9}$$

shown pictorially in Fig. 4. Note that $X(\phi,0)$ also specifies the boundaries of ξ; i.e., $X(-\infty,0)=\xi_1$ and $X(\infty,0)=\xi_N$.

Substituting (9) into (7), it can be shown that

$$\frac{X(\phi,\tau)-\xi_1}{\xi_N-\xi_1}=\frac{1}{2}\left[\sum_{n=1}^{N-1}\frac{\xi_{n+1}-\xi_n}{\xi_N-\xi_1}\mathrm{erf}\left(\frac{(\phi e^{-\tau}-z_n)}{\sqrt{2}a}\right)+1\right]. \tag{10}$$

Taking the derivative of (10) and substituting into (6) finally yields

$$p_\xi(\eta,\tau)=\sigma\left\{\sum_{n=1}^{N-1}(\xi_{n+1}-\xi_i)\times\exp\left[-\frac{(1-\sigma^2)\phi^2-2z_ne^{\tau}\phi+(z_ne^{\tau})^2}{2\sigma^2}\right]\right\}^{-1}, \tag{11a}$$

where $\sigma^2\equiv e^{2\tau}-1=a^2/(1-a^2)$. Recognizing that η represents any value of $X(\phi,\tau)$, (10) implicitly relates ϕ to η in (11a), while

$$z_n=\sqrt{2}\,\mathrm{erf}^{-1}\left(2\sum_{j=1}^{n}D_j-1\right)\quad\text{for}\quad n\in[1,N-1] \tag{11b}$$

follows from (8). Here, $\mathrm{erf}^{-1}(x)$ is the inverse error function.

Extension to the inhomogeneous case can be done following the common method used for the binary mixing problem.[39,40,28,29] This is done by setting, at each computational grid cell, $\xi_1\equiv\xi^-$, $\xi_N\equiv\xi^+$, and obtaining τ for a given σ in (11a), now the statistically stationary PDF of ξ. Physically, ξ^- and ξ^+ represent the respective minimum and maximum local values of ξ in a given computational grid cell and are usually approximated by 0 and 1, respectively. Here, for the general $N>2$ case, to find the unknown parameters for (11a) given ξ^-, ξ^+, and $I>2$ moments at any given point, the $N+1$ generic constraints represented by (5b) are equivalently written as

$$0=\int X^n p_\psi(\phi)d\phi-\langle\xi^n\rangle\quad\text{for } n=0,\ldots,I \tag{11c}$$

using the change of variables of the mapping closure approach. Again, p_ψ here is the standardized Gaussian PDF. The analogous numerical procedure used to obtain $\boldsymbol{C}$ for (5a) can thus be used to solve for the parameters $\boldsymbol{D}=[D_0\ D_1\cdots D_I]^T$, where $D_0\equiv\sigma$ or τ for (11a), the mapping closure model of $p_\xi(\eta)$.

Taking $N=2$ in (11a) retrieves the well-known binary or two-stream mixing problem results of mapping closure. For $N=3$, Ref. 19 results are obtained for the special case $\xi_1=-1$, $\xi_2=0$, $\xi_3=1$, $D_n=1/3$ for all n, and $z_1=-\alpha$, $z_2=\alpha$ (symmetric initial conditions). Application of (11a) for the more general $N=3$ stream DSML case is done next in Sec. V with results compared to the present DNS.

B. Implementation

Implementation of the mapping closure model for the turbulent combustion models reviewed in Sec. II is described.

In contrast to using (2) to obtain the conditional scalar dissipation rate given p_ξ for the CMC and FL modeling approaches, the mapping relation $\xi=X(\phi)$ can instead be used to directly obtain $\langle\chi|\xi=\eta\rangle$ using[14]

$$\frac{\langle\chi|\xi=\eta\rangle}{\langle\chi\rangle}=\frac{\left(\frac{\partial X}{\partial\phi}\right)^2}{\int\left(\frac{\partial X}{\partial\phi}\right)^2 p_\psi(\phi)d\phi}, \tag{12}$$

where $\partial X/\partial\phi$ is the derivative of (10) and p_ψ is given by (11a). Note that the right-hand side of (12) represents $F(\eta)\times(\langle\chi_0\rangle/\langle\chi\rangle)$ following (1a).

For TPDF modeling, Monte Carlo particle simulations of (2) for N streams readily follows the procedure for two-stream mixing described in Ref. 29. Briefly, stochastic differential equations for the notional particles are simulated for the reference field following an Ornstein-Uhlenbeck process:

$$d\psi^{(i)}=-\psi^{(i)}\frac{dt}{T_\psi}+\sqrt{\frac{2}{T_\psi}}\circ dW^{(i)}\quad\text{for}\quad i=1,\ldots,N_p. \tag{13}$$

Here, superscript "(i)" represents the ith notional particle in the ensemble of N_p total particles, $T_\psi=2\langle(dX/d\phi)^2\rangle/\langle\chi\rangle$ is the time scale for ψ, and $W(t)$ is a standard Wiener process. The mapping function (10) is used to obtain $\xi^{(i)}=X(\psi^{(i)})$, whose ensemble then represents the p_ξ of (2).

V. RESULTS AND DISCUSSION

Before turning to the modeling validations of $p_\xi(\eta)$ and $\langle\chi|\xi=\eta\rangle$ for the DSML in Sec. V C below, a physical overview of the DSML is given. The descriptions center around the behavior of the unconditional moments of ξ and χ, their

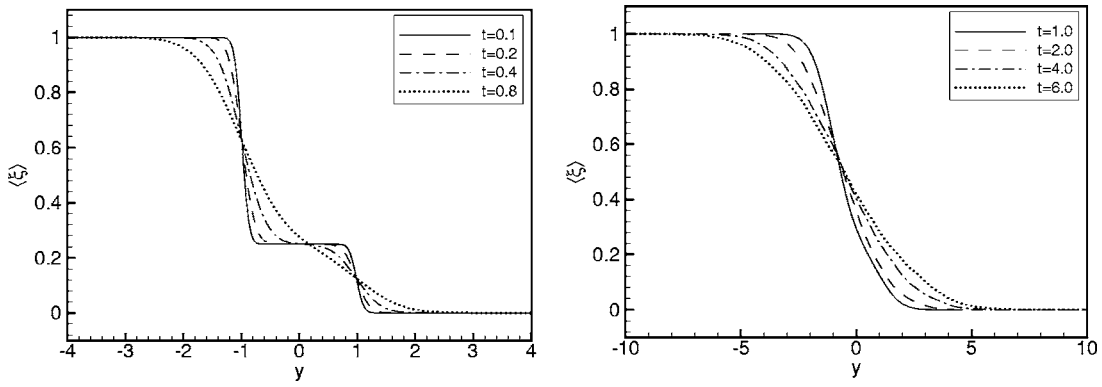

FIG. 5. Profiles of the mean mixture fraction.

existing modeling, and any new physics that would be necessary to model for the particular DSML case versus the well-known, single scalar mixing layer (the binary mixing problem).

A. Moment profiles

Profiles of the mean, rms, skewness (Sk), and kurtosis (Ku) of ξ are plotted in Figs. 5–8 in the nonhomogeneous direction (y) and for various times. The initial premixed region ($\xi=0.25$) of nondimensionalized thickness 2 can be clearly seen in the mean profiles (left subplot of Fig. 5). Due to the two resulting mean scalar gradients, there are two distinct peak locations in the rms profiles (left subplot of Fig. 6). This is a result of scalar turbulence production being proportional to $|\nabla\langle\xi\rangle|^2$. For the DSML, the only nonzero component of this term is $|d\langle\xi\rangle/dy|^2$, which is greatest at these peak locations. That the scalar variance is larger for $y<0$ is due to the larger mean scalar gradient on the fuel ($\xi=1$) side, since $d\langle\xi\rangle/dy\sim\Delta\langle\xi\rangle=(1-0.25)$ is larger as compared to the oxidizer ($\xi=0$) side, where $\Delta\langle\xi\rangle=(0.25-0)$. At comparable times, there are four distinct peaks in the higher moments (Figs. 7 and 8) corresponding to the edges of the two quasi-independent mixing layers of the DSML. These mark the regions of high intermittency that occur at the edge locations of standard, single mixing layers. For increasing times $t\geq 1$ (right subplots of Figs. 5–8), all moments can be seen to become indistinguishable, qualitatively, from a single mixing layer. Note that t is nondimensionalized by the large-eddy turnover time, hence merging of the two scalar mixing layers of $2L_0$ distance in $\mathcal{O}(1)$ time is expected.

The physics behind the first two moments can be described by existing, well-known modeling used in current, standard RANS CFD computations. The expectation is that standard RANS modeling will hence also describe the nonhomogeneous mean and rms fields of the DSML. The turbulence modeling issues of the unclosed terms for the higher moments have not currently been addressed by standard RANS CFD modeling except within the more general TPDF approach, where all moments are computed with the direct computation for the PDF of ξ [cf. (2) and corresponding discussion]. (In Part II of this two-part paper, a method to circumvent solution of these higher moments is described and validated within a combustion modeling framework.)

Temporally, it is useful to divide the evolution of the DSML into three stages. For dimensionless time less than about 0.2, each of the two steps in the double layer behaves approximately independently. At about $t\approx 0.2$, the field enters the second stage of its evolution in which the two layers are not independent, but the effect of the premixed region from the initial condition is strong. This stage lasts until about $t=1$. There are still two distinct peaks in the rms profile, and four distinct peaks in the profiles of the higher moments at this time, but there is no longer a region of nearly zero fluctuations near $y=0$, and the statistics of the fluctua-

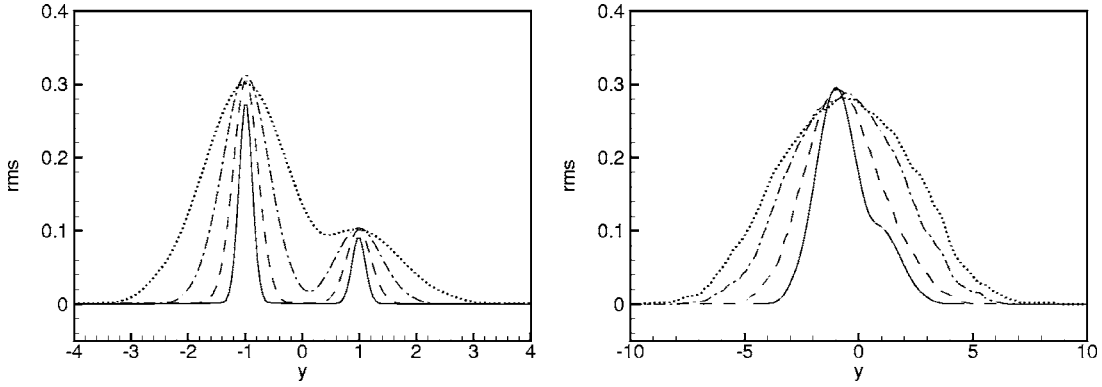

FIG. 6. Profiles of the rms of mixture fraction fluctuations. Line styles are the same as for Fig. 5.

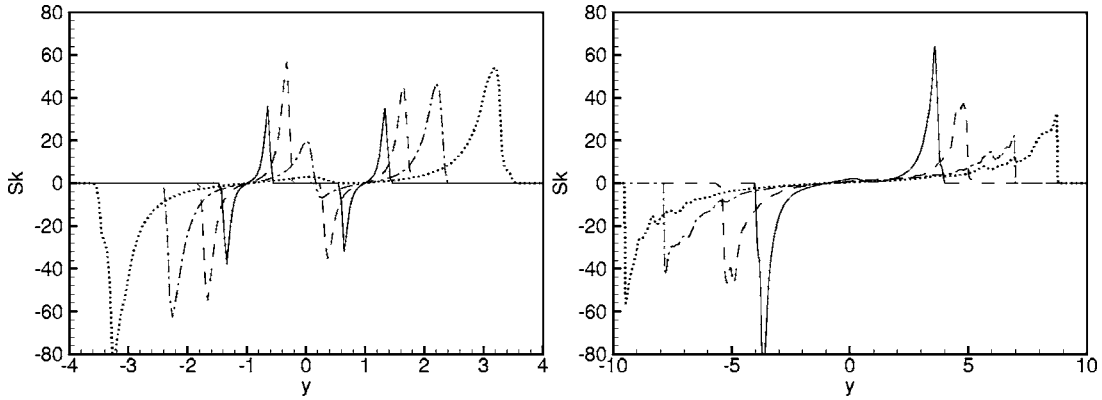

FIG. 7. Profiles of the skewness of the mixture fraction fluctuations. Line styles are the same as for Fig. 5.

tions in ξ change very rapidly near the center of the layer compared with the rate at which they change at other locations in the layer. The flow begins the third and final stage of its evolution shortly after $t=1$. During this time, the effects of the premixed region in the center of the layer are small, and the double layer behaves nearly as a single layer. Beyond $t\approx 1$ then, there is little qualitative difference between the evolution of the DSML and the evolution of the single scalar mixing layer as reported in Ref. 41. As a consequence, we focus on the period $0\leq t\lesssim 1.2$, which encompasses the first two stages in the evolution of the flow, for most of the remaining discussion in this paper.

B. Unconditional dissipation rate

The transverse profile of the unconditional mean of the dissipation rate of ξ is shown in Fig. 9(a). As expected, for $t\lesssim 1.2$, $\langle\chi\rangle$ has a nontrivial, two-peak distribution in y due to the two scalar mixing layers of the DSML. The behavior of the two peaks at these times follow from the physical observations already made above. For example, that the peak of $\langle\chi\rangle$ is greater for $y<0$ is due to the larger scalar variance in the fuel side mixing layer versus the oxidizer side mixing layer. The larger scalar rms is physically indicative of the larger local scalar gradients in the fuel side, whence the larger peak $\langle\chi\rangle$ there. The reason for the larger local scalar gradients in the fuel side is due to the turbulence mixing $\xi=1$ (fuel values) with $\xi=0.25$ versus the mixing of $\xi=0$ and $\xi=0.25$ on the oxidizer side. For a location in the pilot stream, $y=0$, the evolution of $\langle\chi\rangle$ in time is shown in Fig. 9(b). As expected, $\langle\chi\rangle$ starts out as zero due to the uniform $\xi=0.25$ values in the pilot stream, then quickly increases as the turbulence increases the local scalar gradients (i.e., the scalar rms) due to mixing from the fuel and oxidizer streams. During the third, single mixing layer stage of the DSML, $\langle\chi\rangle$ gradually decays.

In the turbulent combustion models (reviewed in Sec. II), the unconditional mean of the dissipation rate of ξ is taken to be known. Kolmogorov's hypothesis of turbulence equilibrium provides the well-known modeling closure for $\langle\chi\rangle$. The present modeling (Sec. IV) also requires $\langle\chi\rangle$ as input. In more advanced turbulent combustion models that account for intermittency effects,[20,27,42] the time-limiting PDF of χ is also of interest. Kolmogorov and Obukhov's hypothesis is generally also adopted for the scalar dissipation, giving

$$p_\chi(\mathrm{X})=\frac{1}{\sigma \mathrm{X}\sqrt{2\pi}}\exp\left[-\frac{(\log \mathrm{X}-\langle\log\chi\rangle)^2}{2\sigma^2}\right], \tag{14}$$

where X is the sample space variable for χ. The σ parameter contains some Reynolds number dependence,[43,44] but in practice, is generally assumed constant.[42,45,46] Note that the value of σ in (14) does not change whether (14) describes χ or χ rescaled/nondimensionalized by some constant value.

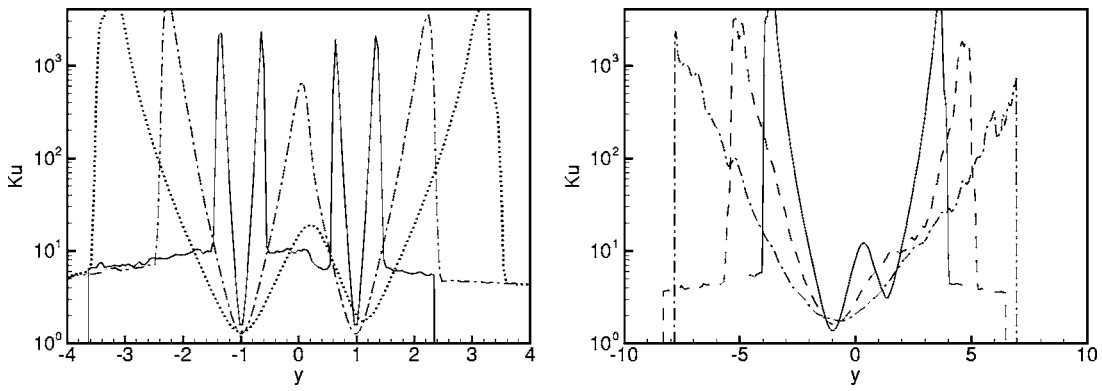

FIG. 8. Profiles of the kurtosis of the mixture fraction fluctuations. Line styles are the same as for Fig. 5, but, for clarity, not as many curves are plotted.

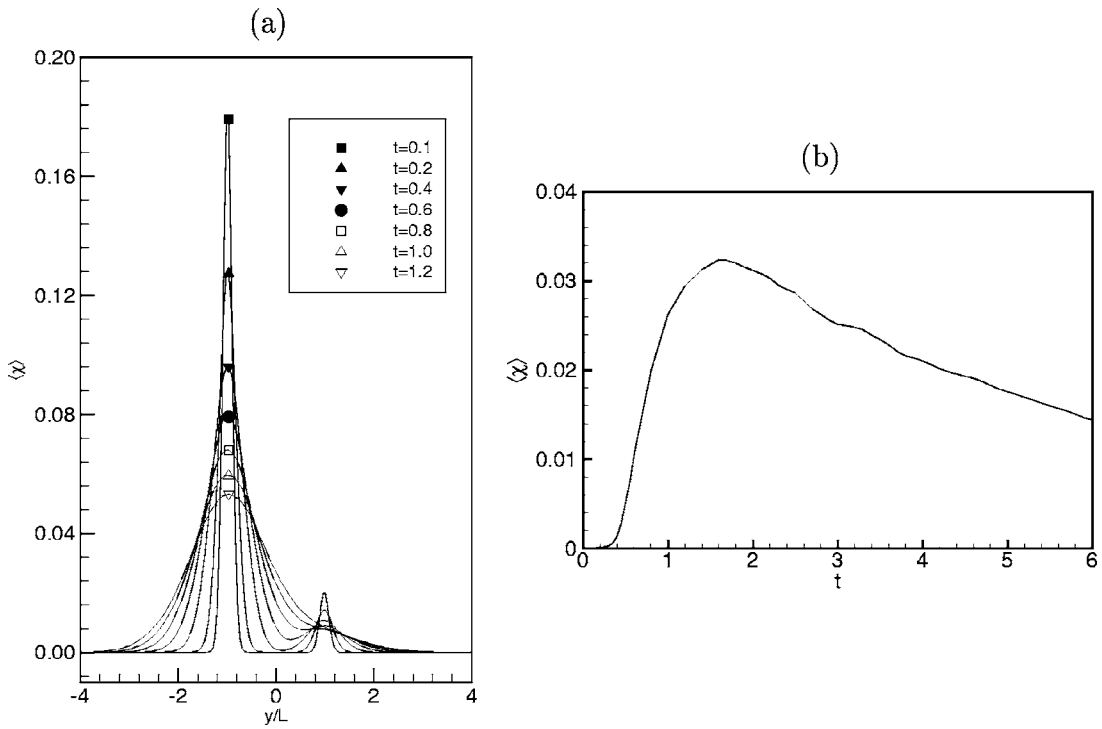

FIG. 9. Profiles of the mean scalar dissipation rate (a) in space and (b) at $y=0$ versus time.

In Fig. 10, the un-normalized PDFs of $\log \chi$ are shown for a range of times and transverse locations. At early time, the PDFs are bimodal, except near the centerline. As the flow evolves, the PDFs tend toward lognormal, but even at $t=6$, (14) is not a particularly good model for $p_\chi(\mathrm{X})$. The figure clearly shows that the conventional method of modeling the distribution of χ with (14), for a single mixing layer, for instance, will not be sufficient even during the late stages of the DSML.

C. Probability density functions and conditional dissipation rates

The probability density of the mixture fraction (p_ξ) and the corresponding conditional scalar dissipation rate ($\langle \chi | \xi = \eta \rangle$) from the DNS are shown by the symbols in Fig. 11 for the nondimensional times of interest ($t \leq 1.2$), and at representative y locations across the mixing layer: Top subplots show the DNS data on the fuel ($\xi=1$) and pilot side at $y=-1.5$; middle subplots in the pilot stream ($\xi=0.25$) at $y=0$; and bottom subplots on the oxidizer ($\xi=0$) and pilot side at $y=0.5$. The data here have been tabulated with equal DNS data points per bin instead of using an equal bin spacing.[47]

Recall that the initial pilot stream spans $-1 \leq y \leq 1$ in physical space, a distance comparable to the largest scale turbulent eddies. Physically, this leads to values of $\xi \approx 0$, which originate from the oxidizer side ($y>1$), to mix by large-scale motions clear across and into the fuel side ($y<-1$). Hence, at $y=-1.5$ for example (top row in Fig. 11), small but nonzero probabilities are observed at low values of η on this fuel side even during these relatively early stages of mixing. As we move to the center of the DMSL, at $y=0$ (middle row in Fig. 11), the mixture fraction PDFs become more equally weighted between the three values of $\eta=0$, 0.25, and 1. This is to be expected as the most equal count of these mixture fraction values should be near the physical origin. Three zero points in $\langle \chi | \xi = \eta \rangle$ are observed at these same η locations. Physically, these points represent the zero gradients of ξ in the pure fuel, oxidizer, and pilot streams, which are then mapped to these same single points in the phase space of ξ. Finally, as we move into the oxidizer side, to $y=0.5$ (bottom row in Fig.11), the probability of finding high, fuel side values of ξ naturally decreases. At all locations at these early times, the shape of $\langle \chi | \xi = \eta \rangle$ with η follows from the observation made in the previous subsections on the approximate decomposition of the DSML into two single (a fuel and pilot and an oxidizer and pilot) mixing layers. As such, two almost independent counterflow distributions can be seen in the η dependence of $\langle \chi | \xi = \eta \rangle$ in Fig. 11; i.e., between $\xi=0$ and 0.25 and $\xi=0.25$ and 1. The corresponding variation of p_ξ with η follows directly from (2). [These observations of $F(\eta)$ for the DSML are exploited in Part II.]

Consistent with the observations of the scalar profiles, the PDFs evolve temporally through three corresponding stages. At early times, the PDF for the entire layer is approximately a triple-delta function with peaks at $\eta=0$, 0.25, and 1, so that, when plotted at a given y value, the initial p_ξ shows a single peak. During the second stage and after a period of time that depends on the y location, the PDF exhibits three peaks at locations near $y=0$ and two peaks at other $|y|>0$ locations. Again, the formation of the second peak reflects

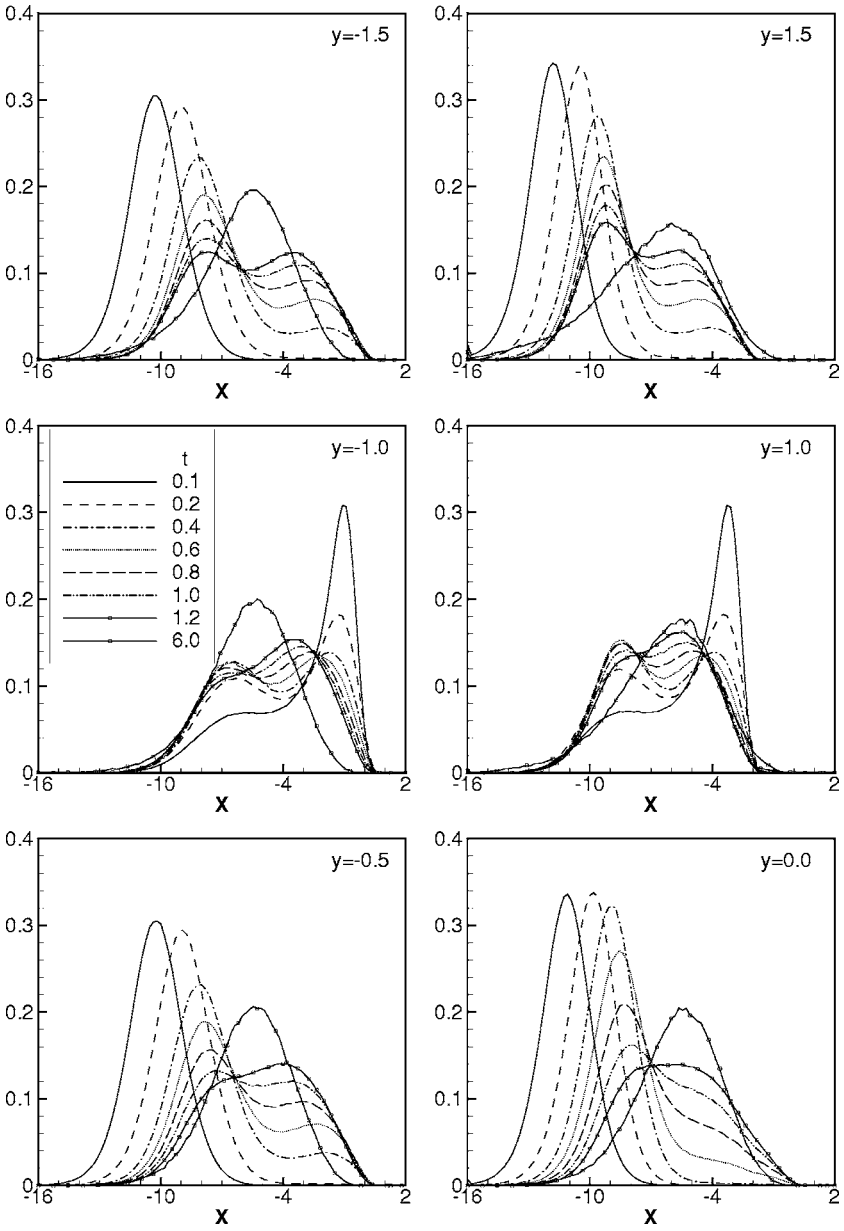

FIG. 10. PDFs of $\log \chi$ from the DNS at six transverse locations and eight times. To make the curves easier to distinguish, the symbols at $t=6.0$ are twice as far apart as at $t=1.2$.

bulk or large-scale stirring of the fluid. At much later times or third stage (not shown), the PDFs at all transverse locations resemble those for a single scalar mixing layer; i.e., the binary mixing problem.

The corresponding mapping closure model results are shown by the lines in Fig. 11. Plotted are (11) and (12) with $N=3$, which then requires the first $I=3$ moments of ξ at a given y location to obtain the mapping closure parameters. Values of ξ^- and ξ^+ are set to 0 and 1, respectively, at all locations in the flow even though $\xi^->0$ or $\xi^+<1$ in regions far away from $y=0$. For example, at $y=-1.5$, values of $\xi=0$ do not exist because it is outside the range of the large-scale turbulence for these times of interest. In spite of this approximation, the mapping closure results are excellent at all times and locations in the mixing layer, validating (10), from which p_ξ and $\langle \chi | \xi=\eta \rangle$ are derived.

VI. SUMMARY AND CONCLUSIONS

Modeling the rate of molecular scalar mixing (χ) is of primary importance for turbulent combustion applications. The response of the heat-releasing chemical reactions to χ determines whether nonpremixed combustion modeling is sufficient or whether more computationally expensive partially premixed modeling need be resorted to. In practice, relations for the unresolved conditional dissipation rate and passive scalar probability distributions provide the necessary information for mixture fraction-based closure modeling such as flamelet modeling and conditional moment closure to describe the temperature, density, and products of chemical reactions. Accurate description of the dissipation rate is also necessary for transported probability density function approaches at the single-point level.

Most practical engineering flows are characterized by

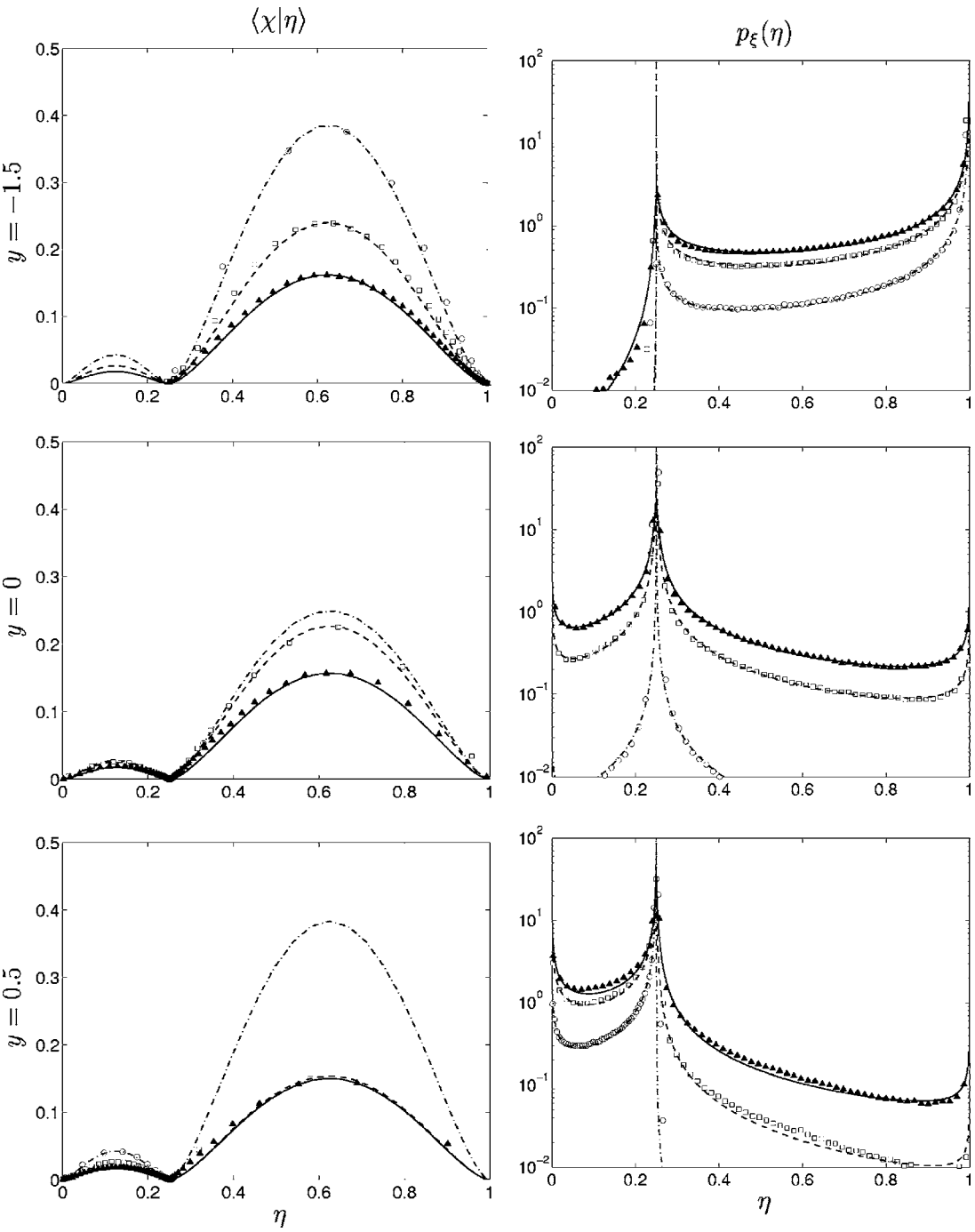

FIG. 11. Comparison of DNS data (symbols) with the mapping closure model (lines) for $\langle\chi|\eta\rangle$ (left column) and $p_\xi(\eta)$ (right column). Each row represents a different y location. Times are $t=0.4$ (circles and dash-dotted lines), 0.8 (squares, dashed lines), and 1.2 (solid triangles, solid lines) in each subplot. Data at $t=1.2$ and $y=0$ are the same as in Fig. 2.

mixing between multiple streams. The double scalar mixing layer (DSML) is a simple model problem which mimics the most essential, multistream mixing behavior by introducing an additional, pilot stream into the classic two-feed or binary mixing problem. High-resolution direct numerical simulations (DNS) are performed to obtain the fine-scale mixing statistics necessary to investigate and develop mixing models that can be applied in the practical configurations.

Comparisons made against the DNS data show that existing standard CFD models, such as the β-PDF, cannot describe the fine-scale passive scalar mixing of ξ in the DSML. Indeed, modeling based on statistical inference alone would require many more moments than just the mean and variance of ξ used to construct the β-PDF. Mapping closure modeling is able to describe the complex PDFs and conditional dissipation rates of the DSML using only the single passive scalar ξ.

ACKNOWLEDGMENTS

High-performance computing resources for this research were provided by the Arctic Region Supercomputing Center.

Financial support for M.M. was sponsored by the Australian Research Council. Special thanks to Prof. R. W. Bilger for his detailed review of the manuscript.

[1]N. Peters, "Laminar flamelet concepts in turbulent combustion," Proc. Combust. Inst. **21**, 1231 (1996).
[2]K. N. C. Bray and N. Peters, "Laminar flamelets in turbulent flames," *Turbulent Reacting Flows* (Academic, New York, 1994), Chap. 2, pp. 63–113.
[3]A. Yu. Klimenko and R. W. Bilger, "Conditional moment closure for turbulent combustion," Prog. Energy Combust. Sci. **25**, 595 (1999).
[4]R. W. Bilger, "Future progress in turbulent combustion research," Prog. Energy Combust. Sci. **26**, 367 (2000).
[5]S. B. Pope, "PDF methods for turbulent reactive flows," Prog. Energy Combust. Sci. **11**, 119 (1985).
[6]C. Dopazo, "Recent developments in PDF methods," *Turbulent Reacting Flows*, edited by P. A. Libby and F. A. Williams (Academic, New York, 1994), Chap. 7, pp. 375–474.
[7]R. S. Barlow, Proceedings of the International Workshop on Measurement and Computation of Turbulent Nonpremixed Flames, Sapporo, Japan, July 18, 2002. http://www.ca.sandia.gov/tdf/Workshop.html.
[8]R. W. Bilger, "Turbulent flows with nonpremixed reactants," *Topics in Applied Physics Number 44: Turbulent Reacting Flows*, edited by P. A. Libby and F. A. Williams (Springer, New York, 1980), Chap. 3, pp. 65–113.
[9]H. Pitsch and H. Steiner, "Scalar mixing and dissipation rate in large-eddy simulations of non-premixed turbulent combustion," Proc. Combust. Inst. **28**, 41 (2000).
[10]S. B. Pope, "Statistical theory of turbulent flames," Philos. Trans. R. Soc. London **291**, 529 (1979).
[11]S. B. Pope, "Probability distributions of scalars in turbulent shear flows," *Turbulent Shear Flows* (Springer, Berlin, 1980), Vol. 2, pp. 7–17.
[12]A. Juneja and S. B. Pope, "A DNS study of turbulent mixing of two passive scalars," Phys. Fluids **8**, 2161 (1996).
[13]H. Chen, S. Chen, and R. H. Kraichnan, "Probability distribution of a stochastically advected scalar field," Phys. Rev. Lett. **63**, 2657 (1989).
[14]E. E. O'Brien and T. L. Jiang, "The conditional dissipation rate of an initially binary scalar," Phys. Fluids A **3**, 3121 (1991).
[15]S. B. Pope, "Mapping closures for turbulent mixing and reaction," Theor. Comput. Fluid Dyn. **2**, 255 (1991).
[16]S. S. Girimaji, "A mapping closure for turbulent scalar mixing using a time-evolving reference field," Phys. Fluids A **4**, 2875 (1992).
[17]F. Gao and E. E. O'Brien, "A mapping closure for multispecies Fickian diffusion," Phys. Fluids A **3**, 956 (1991).
[18]S. S. Girimaji, "A study of multiscalar mixing," Phys. Fluids A **5**, 1802 (1993).
[19]T.-L. Jiang, P. Givi, and F. Gao, "Binary and trinary scalar mixing by Fickian diffusion-some mapping closure results," Phys. Fluids A **4**, 1028 (1992).
[20]C. M. Cha, G. Kosály, and H. Pitsch, "Modeling extinction and reignition in turbulent nonpremixed combustion using a doubly-conditional moment closure approach," Phys. Fluids **13**, 3824 (2001).
[21]H. Pitsch, C. M. Cha, and S. Fedotov, "Flamelet modeling of non-premixed turbulent combustion with local extinction and re-ignition," Combust. Theory Modell. **7**, 317 (2003).
[22]P. A. Libby and F. A Williams, *Turbulent Reacting Flows* (Academic, San Diego, 1994).
[23]E. E. O'Brien, "Probability density function (pdf) approach to reacting turbulent flows," *Topics in Applied Physics*, edited by P. A. Libby and F. A. Williams (Springer, Berlin, 1980).
[24]J. Janicka and N. Peters, "Prediction of turbulent jet diffusion flame lift-off using a PDF transport equation," Proc. Combust. Inst. **19**, 367 (1982).
[25]S. S. Girimaji, "On the modeling of scalar diffusion in isotropic turbulence," Phys. Fluids A **4**, 2529 (1992).
[26]M. Mortensen, "Consistent modeling of scalar mixing for presumed, multiple parameter probability density functions," Phys. Fluids **17**, 018106 (2005).
[27]S. B. Pope, "Computations of turbulent combustion: Progress and challenges," Proc. Combust. Inst. **23**, 591 (1990).
[28]C. M. Cha and P. Trouillet, "A model for the mixing time scale of a turbulent reacting scalar," Phys. Fluids **15**, 1375 (2003).
[29]C. M. Cha and P. Trouillet, "A subgrid mixing model for large-eddy simulations of turbulent reacting flows using the filtered density function," Phys. Fluids **15**, 1496 (2003).
[30]S. M. de Bruyn Kops and J. J. Riley, "Direct numerical simulation of laboratory experiments in isotropic turbulence," Phys. Fluids **10**, 2125 (1998).
[31]S. M. de Bruyn Kops and J. J. Riley, "Re-examining the thermal mixing layer with numerical simulations," Phys. Fluids **12**, 185 (2000).
[32]R. M. Kerr, "Higher-order derivative correlations and the alignment of small-scale structures in isotropic turbulence," J. Fluid Mech. **153**, 31 (1985).
[33]W. E. Mell, V. Nilsen, G. Kosály, and J. J. Riley, "Direct numerical simulation investigation of the conditional moment closure model for nonpremixed turbulent reacting flows," Combust. Sci. Technol. **91**, 179 (1993).
[34]H. Wang and W. K. George, "The integral scale in homogeneous isotropic turbulence," J. Fluid Mech. **459**, 429 (2002).
[35]N. Peters (Private communication).
[36]G. Comte-Bellot and S. Corrsin, "Simple Eulerian time correlation of full and narrow-band velocity signals in grid-generated, 'isotropic' turbulence," J. Fluid Mech. **48**, 273 (1971).
[37]M. Ihme and H. Pitsch, "LES of a non-premixed flame using an extended flamelet/progress variable model," AIAA 43rd Aerospace Sciences Meeting, 2005, AIAA Paper 2005-0558.
[38]F. Gao, "An analytical solution for the scalar probability density function in homogeneous turbulence," Phys. Fluids A **3**, 511 (1991).
[39]A. W. Cook, J. J. Riley, and G. Kosály, "A laminar flamelet approach to subgrid-scale chemistry in turbulent flows," Combust. Flame **109**, 332 (1997).
[40]A. W. Cook and J. J. Riley, "Subgrid-scale modeling for turbulent, reacting flows," Combust. Flame **112**, 593 (1997).
[41]S. M. de Bruyn Kops and M. Mortensen, "Conditional mixing statistics in a self-similar scalar mixing layer," Phys. Fluids **17**, 095107 (2005).
[42]H. Pitsch and S. Fedotov, "Investigation of scalar dissipation rate fluctuations in non-premixed turbulent combustion using a stochastic approach," Combust. Theory Modell. **5**, 41 (2001).
[43]R. W. Bilger, "Some aspects of scalar dissipation," Flow, Turbul. Combust. **72**, 93 (2004).
[44]K. R. Sreenivasan, "Possible effects of small-scale intermittency in turbulent reacting flows," Flow, Turbul. Combust. **72**, 115 (2004).
[45]S. B. Pope and Y. L. Chen, "The velocity-dissipation pdf model for turbulent flows," Phys. Fluids A **2**, 1437 (1990).
[46]C. M. Cha, "Accounting for flamelet structures in conditional moment closure modeling of turbulent combustion," Third Joint Meeting of the United States Sections of the Combustion Institute, March 16–19, 2003, Paper E22.
[47]C. M. Cha and H. Pitsch, "Higher-order conditional moment closure modeling of local extinction and reignition in turbulent combustion," Combust. Theory Modell. **6**, 425 (2002).